Pergamon

Geochimica et Cosmochimica Acta, Vol. 68, No. 14, pp. 3053–3063, 2004

0016-7037/04 $30.00 + .00

doi:10.1016/j.gca.2004.01.017

Long-range vs. short-range ordering in synthetic Cr-substituted goethites

ELSA E. SILEO,[1,*] ALINE Y. RAMOS,[2,3] GRACIELA E. MAGAZ,[4] and MIGUEL A. BLESA[4,5]

[1]INQUIMAE, Departamento de Química Inorgánica, Analítica y Química Física, Facultad de Ciencias Exactas y Naturales, Universidad de Buenos Aires, Pabellón II, Ciudad Universitaria, C1428EHA, Buenos Aires, Argentina
[2]LNLS—Laboratório Nacional de Luz Síncrotron, P,O, Box 6192-CEP 13084-971, Campinas, SP, Brazil
[3]Laboratoire de Minéralogie—Cristallographie de Paris, UMR7590, 75252 Paris Cedex 05, France
[4]Unidad de Actividad Química, Centro Atómico Constituyentes, Comisión Nacional de Energía Atómica, Avenida Gral, Paz 1499, 1650, San Martín, Argentina
[5]Escuela de Posgrado, Universidad Nacional de General San Martín, San Martín, Buenos Aires, Argentina

(*Received February* 13, 2003; *accepted in revised form January* 16, 2004)

Abstract—A series of Cr-substituted goethites with (Cr:Fe molar ratio up to 0.12) were prepared. Thermal analysis of the solids indicates the formation of cation-deficient compounds that are more stable towards the transformation to hematite as the Cr content increases. Powder X-ray diffraction (PXRD) and extended X-ray absorption fine structure (EXAFS) techniques were used to assess the structural characteristics of the whole series of the substituted solids. XRD patterns demonstrate that the order around Fe remains typical of a goethite-like structure. Rietveld refinement of X-ray diffraction data indicates that the incorporation of Cr causes a slight decrease in the cell volume with the *c*-cell parameter following the Vegard's law. This decrease is accompanied by changes in opposite directions of the various Me-Me distances. EXAFS spectra at the Fe K-edge indicate that the local order around the Fe atom changes slightly upon Cr substitution: Measurements in the Cr K-edge show that the Cr environment remains unchanged in the whole series. All the observed trends in both average Rietveld and local EXAFS distances can be traced back to the differences in the coordination polyhedra around Cr and Fe. The polyhedron around Cr is more symmetric and can be described as $Cr(OH_{0.5})_6$ as opposed to the polyhedron around Fe that contains two distinct sets of ligands, $FeO_3(OH)_3$. The effects caused by substitution are governed by this difference, rather than by the smaller size of Cr(III) as compared to Fe(III). Simultaneous use of XAS and Rietveld refinement of XRD data permits tracing the trends in the average long range ordering (Me-Me distances) to local changes in distances and angles when Cr^{3+} substitutes Fe^{3+} in goethite. Complex changes in the various interatomic distances and angles may result in deceivingly simple long-range trends. These trends are therefore of limited value as probes for the atomic scale changes. On the other hand, XAS provide direct information on the fundamental, atomic-scale changes.

1. INTRODUCTION

Many minerals on the earth's surface, especially in tropical and subtropical regions, are nonsilicate minerals, namely Fe and Al oxides. Goethite (α-FeOOH) is one of the iron oxides produced by the weathering of various nonsilicate and Fe-containing silicate minerals; it imparts soils with a characteristic yellow-brown color. For more information on the mineralogy and chemistry of Fe oxides in soils, see Schwertmann (1988).

Under anaerobic conditions, the solubility of Fe and Mn oxides is higher as compared with that of aluminosilicates; this fact favors coprecipitation and solid solution formation with different metal ions. Oxides reduction in soils generates soluble Fe(II) and Mn(II) salts that reoxidize when the soil is aerated, to form again the insoluble oxides. During these cycles of alternating reduction and oxidation, coprecipitation of trace metals often takes place (Blesa and Matijevic, 1989; Blesa et al., 1994; Domingo Pascual et al., 1994; McBride, 1994).

Although its abundance in soil may vary between 1 and 5%, goethite surfaces may account for an important fraction of the total surface area (Schwertmann and Taylor, 1989). Small-grained goethite is highly reactive for surface adsorption and complexing (Spadini et al., 1994; Cornell and Schwertmann, 1996; Parkman et al., 1999). Because of its abundance and surface reactivity, goethite plays an important role in aqueous geochemistry and it is an efficient scavenger for metals. Soil goethite is seldom pure and may contain significant amounts of aluminium; manganese and other trace metals are also frequently associated with goethite (Norris and Taylor, 1961; Lewis and Schwertmann, 1979; Norris and Rosser, 1983; Stiers and Schwertmann, 1985; Cornell and Schwertmann, 1996, and references therein; Parkman et al., 1999).

Chromium is widely used in the steel industry, and in the production of heat-resistant and chemically resistant bricks, pigments, electroplating, and in the dye, tanning, textile and chemical industries (Faust and Aly, 1981; Moore and Ramamoorthy, 1984). Because of its widespread use, chromium may be easily released into the environment. Soil conditions generally favor the formation of Cr(III) soluble species by complexation with organic matter. These species may become immobilized by chemisorption on oxides and silicate clays, even at quite low pH. Furthermore, Cr^{3+} readily substitutes for Fe^{3+} in mineral structures, and precipitates as insoluble hydrous chromium(III) oxide at higher pH (Baes and Mesmer, 1976).

Many minerals contain Cr(III). Bracewellite, CrOOH (Milton et al., 1976) is isostructural with goethite. The surface of

* Author to whom correspondence should be addressed (sileo@qi.fcen.uba.ar).

goethite may be include attached Cr(III) ions which were released from Cr-bearing minerals during weathering. It is not clear however if substituted goethite may originate from preformed goethite containing adsorbed Cr(III), by diffusion, or whether incorporation in the lattice framework must take place in ferrihydrite, before crystallization to goethite. In any case, Cr(III) substituted goethites are found in nature. The ionic radius of Cr(III) is slightly smaller than that of Fe(III) (0.615Å vs. 0.645Å), and substitution causes a small reduction in the unit cell parameters of goethite (Schwertmann et al., 1989).

Powder X-ray diffraction (PXRD) data have been used to explore the structure of substituted goethites. As a part of his comprehensive study by powder diffraction, Schwertmann et al. (1989), have reported that the changes in the *a*- and *c*-parameters in Cr-substituted goethites are in agreement with Vegard's law, whereas *b* largely deviates from Vegard's predictions. It is clear however that data processing by procedures such as Rietveld simulation (Rietveld, 1969), is required to extract good structural information. Although single crystal XRD is an accurate tool for structural determination, its usage has been limited in the past by the lack of large crystals. This is no longer a limitation with the advent of third generation synchrotron sources.

The purpose of this work is to explore the structure of chromium substituted goethites by a combination of a method sensitive to long-range order, namely powder X-ray diffraction (PXRD), and a method sensitive to short-range atomic order, namely X-ray absorption spectroscopy (XAS). The changes in unit cell parameters are expectedly small due to the small differences in Cr(III) and Fe(III) ionic radii. Therefore, long-range order structural changes were calculated by the Rietveld simulation of experimental data, as this method permits accurate determination of unit-cell parameters. This method also provides the atomic parameters required to calculate Fe-Me distances. XAS, including EXAFS (extended X-ray absorption fine structure) and XANES (X-ray absorption near edge structure) spectroscopies provide complementary data describing the local arrangement about the Fe and the Cr ions separately. XAS has already been used to study the (isomorphous) substitution in Ga- (Martin et al., 1997) and Mn-inserted goethites (Scheinost et al., 2001), the distribution of Fe in Fe-inserted diaspore (Hazemann et al., 1992), the oxidation state and the short-structural order of Mn in a Mn-containing goethite (Manceau et al., 1992a,b), and the substitution and inter or over-grown domains in oxides (Manceau and Combes, 1988; Charlet and Manceau, 1991; Manceau et al., 2000).

2. MATERIALS AND METHODS

2.1. Sample Preparations and Analysis

Goethite was prepared as described by Schwertmann and Cornell (1991) by adding 100 mL of a 1 mol/L $Fe(NO_3)_3$ solution to 180 mL of a 5 mol/L KOH solution. The suspension thus obtained was diluted to 2 L with double-distilled water and aged for 60 h at 70°C in a closed polyethylene flask. The final product was filtered, washed with double-distilled water and dialyzed until the conductivity of the solution was similar to that of double-distilled water. The solid was dried at 50°C for 48 h and then gently crushed.

Cr-substituted goethites were also prepared following Schwertmann and Cornell (1991), by aging at 70°C, in closed polyethylene flasks, mixtures of 0.3 mol/L KOH solutions containing respectively 1 mol/L $Fe(NO_3)_3$ and 0.18 mol/L $Cr(NO_3)_3$, in the adequate volume ratio to yield the desired μ_{Cr} ratio (μ_{Cr} = [Cr] × 100/[Cr] + [Fe], [Me]: mol L^{-1}). Four suspensions were prepared, with initial μ_{Cr} values of 0.032, 0.072, 0.134 and 0.265, respectively. After 153 d, the suspensions obtained were filtered and amorphous materials were removed from the solid by treatment with a 2 mol/L H_2SO_4 solution at 80°C for 2 h. The same washing, dialyzing and drying procedures were used as those for pure goethite.

Grimaldiite, α-CrOOH, was synthesized hydrothermally, by treating a 0.3 mol/L $Cr(NO_3)_3$ solution at 200°C and 2.5 MPa during 1 h. After cooling, the resulting suspension was filtered, and the solid was washed several times with double-distilled water and dialyzed as described before. Reagent grade chemicals were used for all syntheses.

The Fe and Cr contents in the samples were determined by X-ray fluorescence. Complementary, semiquantitative energy dispersive X-ray analysis (EDS) was performed to search for regions of different compositions. Particle morphology and size were characterized using scanning electron microscopy (SEM). Samples for SEM were dispersed in double-distilled water using an ultrasonic bath and a drop of this suspension was placed onto a metallic support. SEM images and EDS data were obtained in Philips SEM 515 equipment operated at 30 keV.

Thermogravimetric (TGA) and differential thermal analysis (DTA) were performed using a TGA-51 and a DTA-50 Shimadzu instrument, respectively. Samples of ~20 mg (for TGA measurements) and 6.0 mg (for DTA measurements) were heated in a N_2 atmosphere in the temperature range 30–1100°C (heating rate 6°C/min).

Diffraction patterns were recorded in a Siemens D5000 diffractometer in a Bragg-Brentano geometry, using Cu Kα radiation. Generator settings were 40 kV, 30 mA. Divergence, scattered and receiving radiation slits were 1°, 1° and 0.2 mm, respectively. A graphite monochromator was used. Data were collected in the 2θ range: 15.800–140.000°, with scanning step of 0.025° and counting time of 20 s per point. The data were analyzed using the GSAS (Larson and Von Dreele, 1994) system.

2.2. X-ray Diffraction Refinement

The whole X-ray diffraction pattern was used to refine the crystal structure. Only isotropic atomic displacements were considered. Starting unit-cell parameters and atomic coordinates for goethite were taken from the literature (Szytula et al., 1968). A fraction of Cr ions, defined by the chemical analysis data, was initially placed in the Fe positions, and the total occupancy factor for the metal site was refined. The measured background was fitted by a simple linear interpolation formula. Peak profiles were fitted using the Thompson-Cox-Hastings pseudo-Voigt function (Thompson et al., 1987) with the microstrain broadening description of Stephens (1999). Cell parameters and sample displacement, full width at half maximum, microstrain broadening parameters for the peak shape, scale factor, positional and isotropic thermal parameters for all atoms were also refined. The preferred orientations were corrected in all samples by the March model (Dollase, 1986).

2.3. XAS Data Collection and Analysis

The XAS spectra of grimaldiite and goethite were collected at the chromium (5989 eV) and iron (7112 eV) K-edges, respectively. The spectra of the Cr-inserted goethite samples were collected at both edges. Several spectra (four to six) were averaged for each sample.

X-ray absorption measurements were performed at the XAS beam line of the Laboratório Nacional de Luz Síncrotron (LNLS, Campinas, Brazil) (Tolentino, 2001). The LNLS storage ring operates at 1.37 GeV with nominal current of 130 mA. X-ray absorption data were collected in the transmission mode using air-filled ion chambers. The incident beam was monochromatized with a "channel-cut" Si (111) monochromator. The overall energy resolution, including core hole and experimental resolution is 3.0 eV at the Fe-K-edge and 2.8 eV and 1.6 eV at the Cr K-edge for EXAFS and XANES, respectively. The energy was calibrated at the inflexion point of edge jump in the XANES spectrum of metallic foil (7112 eV at the iron edge, 5989 eV at the chromium edge). Cr-and Fe K-edge EXAFS spectra were collected in the range 5900 to 6900 eV and 7040 to 7800 eV, respectively, with energy steps of 2 eV. The XANES spectra were collected in the range 5970 to 6050 eV with an energy step of 0.5 eV and the background was corrected

Table 1. Molar chromium and water content of the solids; derived atomic composition shown in the last column.

Sample	μ_{Cr} (initial)	μ_{Cr} (XRF)	μ_{Cr} (EDS)	H_2O % (stoichiometric)	DTA peak	α-$(Fe_{1-x}Cr_x)_{1-y/3}O_{1-y}(OH)_{1+y}$
C1	0	0	0	10.26 (10.13)	288.0	α-$Fe_{0.996}O_{0.989}(OH)_{1.011}$
C2	3.9 ± 0.1	4.31 ± 0.01	4.1 ± 0.2	11.31 (10.14)	304.9	α-$Fe_{0.927}Cr_{0.042}O_{0.906}(OH)_{1.094}$
C3	7.2 ± 0.1	7.26 ± 0.15	7.1 ± 0.4	13.13 (10.16)	312.0	α-$Fe_{0.851}Cr_{0.067}O_{0.756}(OH)_{1.249}$
C4	13.4 ± 0.2	10.22 ± 0.20	10.1 ± 0.5	11.92 (10.17)	314.6	α-$Fe_{0.856}Cr_{0.097}O_{0.861}(OH)_{1.139}$
C5	26.5 ± 0.2	12.42 ± 0.25	12.2 ± 0.5	11.44 (10.18)	314.5	α-$Fe_{0.846}Cr_{0.120}O_{0.899}(OH)_{1.101}$

using a polynomial fit in the region before the preedge and then normalized close to 6050 eV.

The EXAFS spectra were analyzed using a standard data reduction procedure (Sayers and Bunker, 1988), using WinXAS version 2.2 (Ressler, 1997). The preedge absorption was fitted and extrapolated to the whole energy range. The edge position was taken at the inflection point of the edge jump. The EXAFS oscillations, χ(k), were extracted by subtracting the spectra from a fitted smooth polynomial function. The k-weighted EXAFS signal, kχ(k), was then filtered by a Bessel function and Fourier transformed into the *R*-space. The modulus of the Fourier transform shows maxima generated by the shells of the scattering atoms surrounding the absorbing atom. The positions of the peaks in |F(r)| are shifted compared to the true distances. These shifts are related to an additional phase which accounts for the influence of the potential of the absorbing atom and the scattering atoms on the electron wave. The contribution of each shell was then back-transformed to the k-space.

Theoretical paths were calculated with ATOMS and FEFF 7.02 code (Rehr et al., 1991), using the structures obtained through our own Rietveld refinements. The full structure out to 6.5 Å was used as FEFF input to obtain correct potentials. The short-range structure around Cr and Fe was modelled by multishells fits. The amplitude reduction factors S_0^2 in FEFF calculations were set to 0.85 and 1 for the Me-O and Me-Me shells, respectively. These parameters were calibrated from reference compounds, namely, goethite and grimaldiite. A single value of E was varied in each shell. Parameters allowed to float in fits at the Fe- and Cr-edges were interatomic distances ($R_{Me\text{-}O}$, $R_{Me\text{-}(Fe,Cr)}$), Debye-Waller factors or disorder parameters ($\sigma^2_{Me\text{-}O}$, $\sigma^2_{Me\text{-}Me}$) and the difference between the threshold energy (E_o) relative to FEFF phase shift function (ΔE). In some cases the coordination numbers ($CN_{Me\text{-}O}$, $CN_{Me\text{-}(Fe,Cr)}$) were also refined.

3. RESULTS AND DISCUSSION

3.1. Chemical and Physical Analysis of the Solids

Table 1 shows the values of μ_{Cr} for the synthesized solids, as measured by X-ray fluorescence (XRF); the initial solution values and the semiquantitative EDS analysis data are also shown. For samples C_2 and C_3, μ_{Cr} in the final solid is higher than in the initial solution, indicating that the amorphous phases removed by extraction with 2 mol/L H_2SO_4 at 80°C are depleted in Cr(III). The plateau in the uptake of Cr at high [Cr(III)] is probably dictated by the solubility limit in the goethite structure. Table 1 also shows the water content up to 1100°C, measured by the mass loss in TGA experiments according to the following equation; stoichiometric values (y=0) are shown in parenthesis.

$$2\alpha\text{-}(Fe_{1-x}Cr_x)_{1-y/3}O_{1-y}(OH)_{1+y} \rightarrow (1 - y/3)\alpha\text{-}(Fe_{1-x}Cr_x)_2O_3 + (1 + y)H_2O,$$

Heating in the temperature range of 30–140°C eliminates absorbed water. According to TGA measurements, this water does not exceed 1 wt% in all samples. Structural water, which defines the OH^-/O^{2-} ratio, is eliminated in the range from 140–1100°C. In all samples, this ratio exceeds the value of 1 typical of stoichiometric α-FeOOH (H_2O wt. = 10.13%). Accordingly, the total metal content (1-y/3) corresponds to metal-deficient goethites (y > 0). Similar features have been reported for the Al-inserted goethites (Wolska and Schwertmann, 1989).

Figure 1 shows the DTA traces. The endothermic peak corresponding to the structural water released from the OH^- groups is displaced to higher temperatures when the Cr content increases. The same feature was observed for Al-substituted goethites (Schulze and Schwertmann, 1984).

The XRD patterns of the five samples point to a goethite-like structure; no other phase is detected. Small changes in peak positions indicate slight changes in the unit cell parameters for the Cr-inserted samples. The quality of fit of the XRD data is discussed below.

3.2. Crystal Morphology

Figure 2 shows SEM micrographs for different samples. All particles are acicular. For C2, a minor quantity of spherical particles is also observed. Cr is the only metal detected by EDS analysis in these latter particles. The results suggest a small degree of segregation of an amorphous $Cr_2O_3.xH_2O$ phase. This is consistent with the slightly different C2 XANES pattern (see below).

The particles of substituted goethites are, in all cases, smaller than those of nonsubstituted α-FeOOH. The length L of the

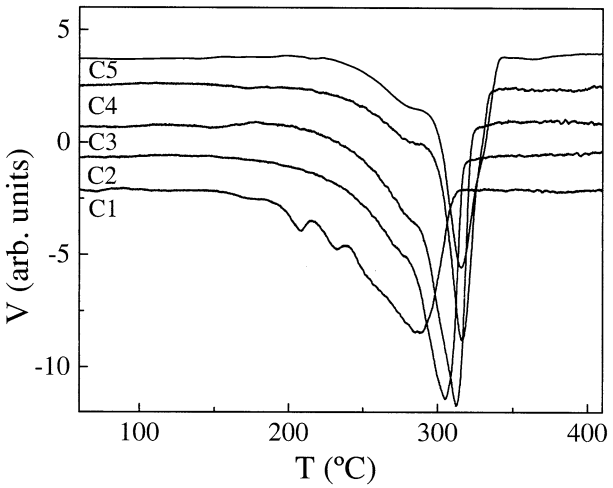

Fig. 1. DTA traces for goethite and Cr-substituted goethites. Cr contents indicated in Table 1.

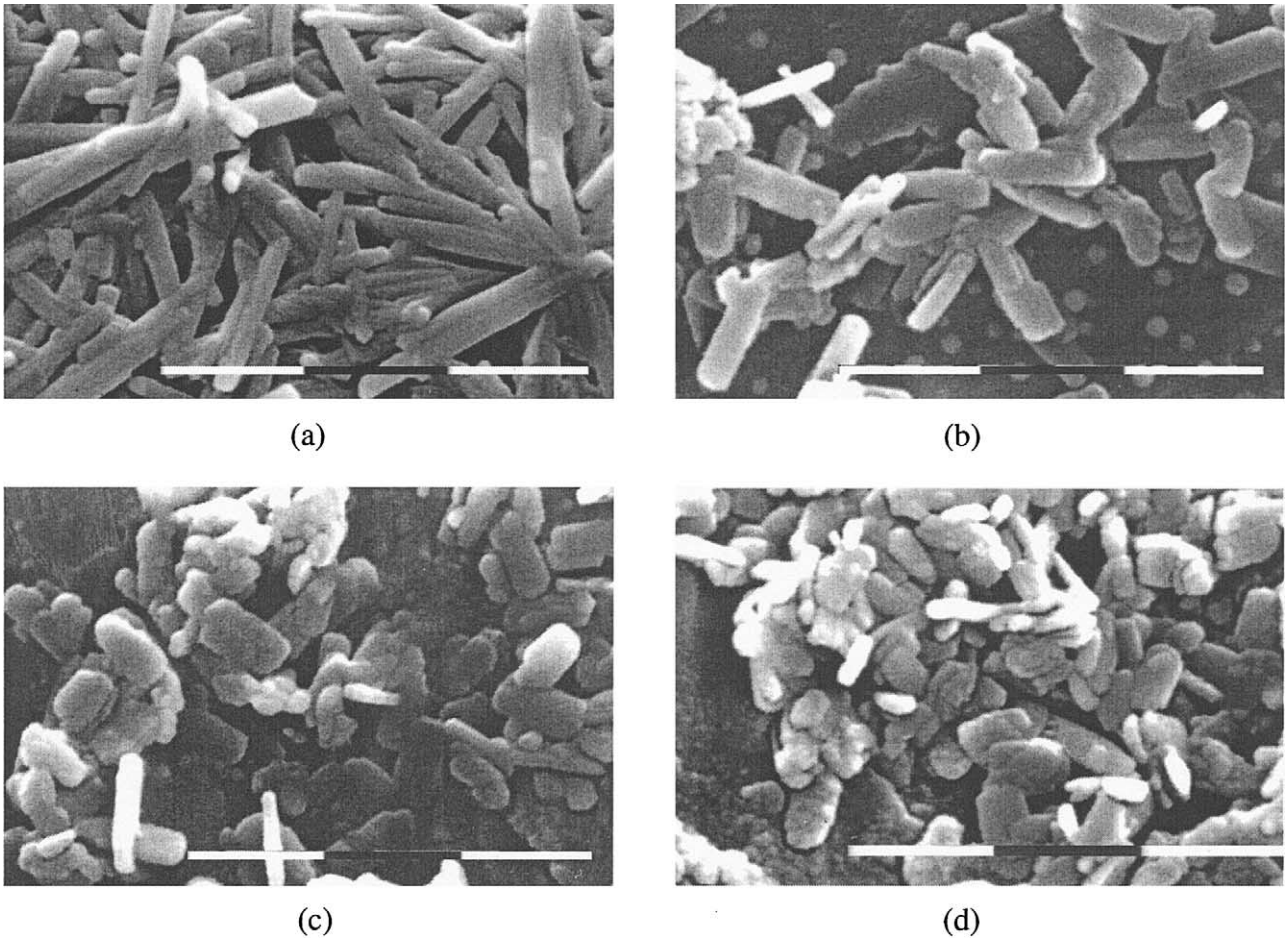

Fig. 2. SEM micrographs of samples (a) C1, (b) C2, (c) C3 and (d) C4. Abbreviations in the text (scale 1 div = 1 μm).

substituted acicular particles display a range from $0.6 \leq L \leq 1$ μm, whereas for α-FeOOH, $L \cong 2$ μm. The width-to-length ratio increases with increasing Cr substitution. The formation mechanism of the acicular particles is known to involve the oriented aggregation of much smaller crystallites (Blesa and Matijevic, 1989; Domingo Pascual et al., 1994). In this interpretation, chromium's effect is to hinder oriented aggregation thus producing less perfect particles with a smaller aspect ratio. Sileo et al. (2001) have observed the opposite trend in Mn-substitution in goethite.

3.3. Rietveld Refinement of XRD Data

Table 2 collects the parameters that describe the goodness of the fitting for the various samples. The quality of the refinement is similar for the five samples; reliability factors are in the range Rwp = 7.48 − 9.15; R_B = 3.22 − 5.20, GofF values are reasonably adequate, between 1.08 − 1.35.

Several values of the preferred orientation function have been used during the refinement, but only those corresponding to the 021 and 040 orientations improved markedly the quality of the refinements. In all samples, the refined metal (Fe,Cr) occupancy factor is smaller than 1.0, in agreement with the metal deficiency detected by the TGA analyses.

Figure 3 compares the experimental and the calculated diffraction patterns for sample C3, and shows that the selected goethite-like structural model fits the experimental data well.

3.4. Structural Change and Lattice Parameters of Substituted Samples

Lattice parameters and cell volume obtained in the Rietveld refinement of the various samples are shown in Table 3 and Figure 4.

Table 2. Agreement factors for the refinements.

Sample	Rwp	Rp	GofF	R_B
C1	7.48	5.69	1.08	3.22
C2	8.75	6.82	1.26	3.50
C3	8.77	6.87	1.24	4.32
C4	9.15	7.32	1.35	5.20
C5	8.48	6.62	1.23	4.08

Rp: $100\ \Sigma\ |I_o - I_c|/\Sigma\ I_o$. R_B: $100\ \Sigma\ |I_{ko} - I_{kc}|/\Sigma\ I_{ko}$. Rwp: $100\ [\Sigma\ w_i\ (I_o - I_c)^2/\Sigma\ w_i\ I_o^2]^{0.5}$. GofF = $\Sigma\ w_i\ (I_o - I_c)^2/(N - P)$. I_o and I_c: observed and calculated intensities. w_i: weight assigned to each step intensity. I_{ko} and I_{kc}: observed and calculated intensities for Bragg k-reflection. N and P: number of data points in the pattern and number of parameters refined.

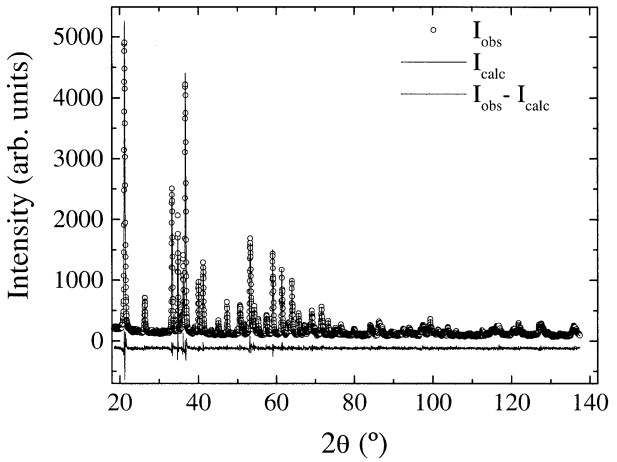

Fig. 3. Observed (◦), calculated (−), and difference final profiles for the Rietveld refinement of C3.

All cell parameters decrease upon increasing substitution, the *c*-parameter following approximately the Vegard's law. At low degrees of substitution, the *b*-parameter also behaves as predicted by Vegard's law, but it remains roughly constant at larger substitution degrees (Fig. 4b). The behavior of *a*- is opposite: small changes occur at low substitution degrees, larger changes occur as substitution increases, followed with an approach to the value predicted by the Vegard law by the sample with the largest degree of substitution (Fig. 4a). The cell parameters of several samples of Cr-substituted goethites calculated from six diffraction peaks (Schwertmann et al., 1989) gave similar features.

In the goethite structure, half of the octahedral sites of the HCP packing of oxide and hydroxide groups are filled with metal ions (Szytula et al., 1968). Goethite is orthorhombic, space group Pnma (Z = 4); however, it is usually described using the Pbnm group. To facilitate comparisons with previous works, we present the refinement results using the Pbnm group.

The structure consists of double rows or ribbons of edge-sharing Fe octahedra that run parallel to [001]; these double rows are separated by vacant double rows of channels that also run along [001]. The double rows are formed by polyhedra that share two hydroxide groups. The ribbons along [001] are formed by the connection of polyhedra that share one oxide and one hydroxide group from the same edge. Double ribbons, connected through the corners by oxide groups, complete the

Table 3. Lattice cell parameters for samples C1 to C5.[a]

Sample	*a* (Å)	*b* (Å)	*c* (Å)	Volume (Å^3)
C1	4.6094 (2)	9.9587 (2)	3.02384 (7)	138.805 (8)
C2	4.6089 (1)	9.9543 (1)	3.02066 (4)	138.585 (4)
C3	4.6072 (1)	9.9547 (1)	3.01989 (4)	138.501 (3)
C4	4.6016 (2)	9.9538 (2)	3.01845 (7)	138.256 (4)
C5	4.5971 (1)	9.9526 (2)	3.01766 (6)	138.069 (8)

[a] Values in parentheses are esd for the least significant figures of the data shown, the esd values are taken from the final cycle of the Rietveld refinement.

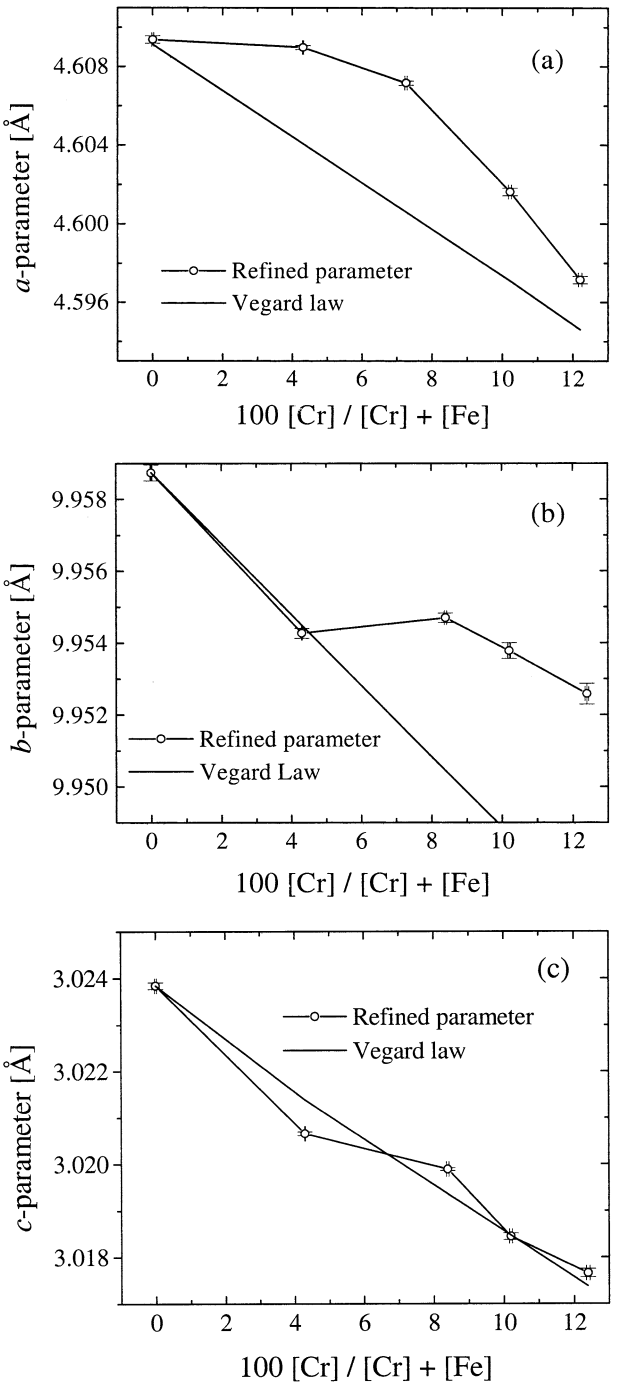

Fig. 4. Lattice parameters vs. cr content in the samples.

structure. Three different Fe-Fe distances characterize the structure. Within each double row, there are two different distances between the Fe atoms of adjacent, edge-joined polyhedra, depending on the nature of the groups in the corners of the edge. These distances are labeled E (two OH groups in the corners of the edge) and E′ (one O and one OH group in the corners of the edge), E′ coincides with the *c*-parameter. The connection between double rows determines another Fe-Fe

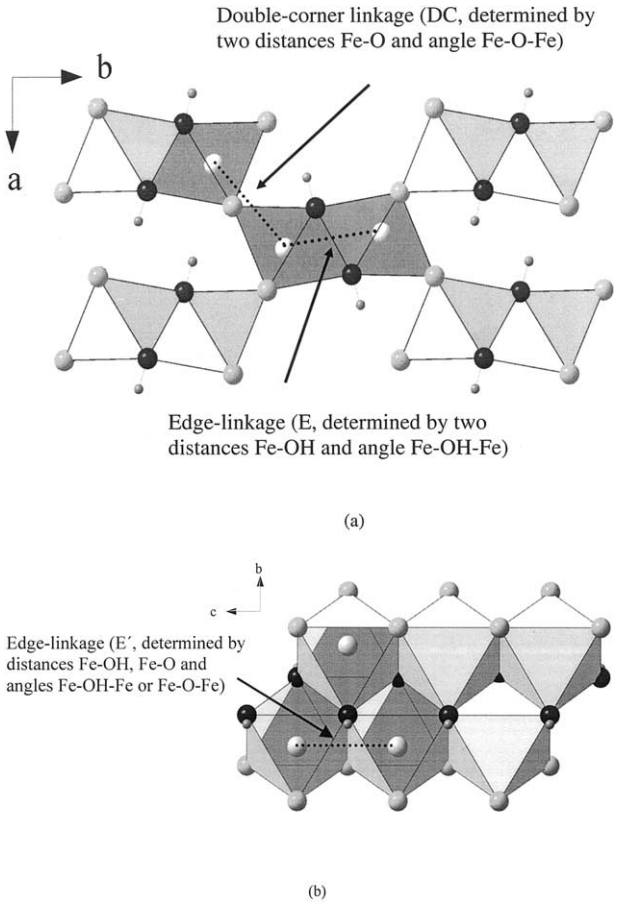

Fig. 5. Goethite structure showing the polyhedra linkage: (a) (001) and (b) (100) directions.

distance, named a DC (double corner) distance (determined by the Fe-O distance and the Fe-O-Fe angle). These features are shown in Figure 5.

Table 4 shows the refined (x,y) atomic parameters for (Fe,Cr), O1 (oxide oxygen) and O2 (hydroxide oxygen); note that $z = 0.250$ in all three cases. The moduli of x(Fe,Cr) and y(Fe,Cr) decrease in the Cr-substituted samples; x and y for O1 and O2 remain essentially constant. Table 5 shows that the calculated E and E′ distances decrease slightly along the series, whereas DC remains essentially constant, and even increases slightly in going from C1 to C5, even though the cell shrinks; thus, Cr incorporation produces an anisotropic distortion in the cell. This effect must be attributed to the distortion of the $Me(OOH)_6$ polyhedra. The trend in E′ (that coincides with c, see Fig. 4c) is in line with the overall decrease in cell dimensions when the Cr content increases.

Table 5. Calculated Me-Me distances in the series.

Sample	E (Å) (two distances)	E′ (Å) (two distances)	DC (Å) (four distances)
C1	3.310 (2)	3.0238 (1)	3.446 (1)
C2	3.303 (2)	3.0207 (1)	3.448 (1)
C3	3.300 (2)	3.0199 (1)	3.450 (1)
C4	3.296 (2)	3.0185 (1)	3.449 (1)
C5	3.292 (2)	3.0177 (1)	3.450 (1)

The absolute values of the parameters and distances shown in Tables 4 and 5 for C1 cannot be compared directly with the data reported for goethite single crystals, and reflect the synthetic procedure used to prepare the powders. No previous data of atomic parameters in Cr-substituted goethites could be found in the literature.

3.5. Local Order around Fe(III)

The EXAFS spectra of C1, C2 and C5 at the Fe K-edge are shown in Figure 6; k^3-weighted signals are shown to enhance possible differences. Spectra are slightly dissimilar indicating small changes in the coordination shells of the absorbing atom.

The Fourier transform (FT, modulus and the imaginary part) of the k-weighted χ(k) are presented in Figure 7 for samples C1 and C5. Since the Fourier transforms are not phase-shift corrected, peak positions do not represent the true distances. The first peak corresponds to the oxygen shell surrounding the absorber (Fe-O); the second and the third peaks correspond to the sum of three different Fe-Fe,Cr contributions (Charlet and Manceau, 1991; Manceau and Drits, 1993), two Fe-Me_1, two Fe-Me_2 and four Fe-Me_3 interactions at distances E′, E and DC, respectively. The second peak in the spectra is attributable mainly to the E′ interaction, whereas the location of the maximum of the third peak suggests that it results from the averaging of unresolved E and DC contributions.

The signals of the first (oxygen) coordination shell do not change much upon substitution. On the other hand, the signal associated with E′ links moves to smaller distances, and the mixed signal from the E + DC shells moves to larger distances; in both cases, the displacements are small.

To analyze the variation of the local environment around Fe shown in Figure 7, the three peaks in the ranges 0.9–2.0, and

Table 4. Atomic parameters for the Cr-inserted goethites.[a]

Sample	x(Fe,Cr)	y(Fe,Cr)	x(O1)	y(O1)	x(O2)	y(O2)
C1	0.0478 (2)	−0.1462 (1)	−0.2879 (7)	0.1981 (3)	0.1939 (6)	0.0537 (3)
C2	0.0483 (2)	−0.1459 (1)	−0.2923 (8)	0.1994 (3)	0.2008 (7)	0.0526 (3)
C3	0.0480 (2)	−0.1457 (1)	−0.2924 (9)	0.1991 (3)	0.2022 (7)	0.0533 (3)
C4	0.0477 (2)	−0.1455 (1)	−0.2922 (9)	0.1991 (4)	0.2020 (8)	0.0530 (4)
C5	0.0476 (2)	−0.1453 (1)	−0.2916 (9)	0.1985 (4)	0.2000 (7)	0.0537 (3)

[a] Values in parentheses are esd for the least significant figures of the data shown, the esd values are taken from the final cycle of the Rietveld refinement.

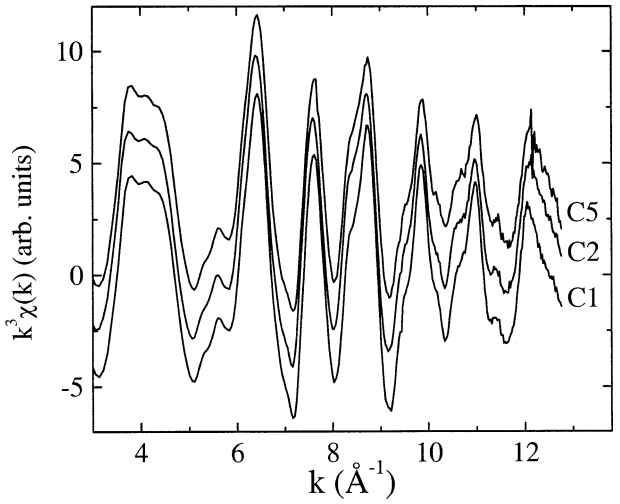

Fig. 6. k^3-weighted EXAFS spectra of C1, C2 and C5 at the Fe K-edge.

2.2–3.6 Å were isolated, backtransformed and analyzed in k^3-space in the range $3.5 < k < 12.8$. As noted, the average distances to O^{2-} and OH^- ions remain constant in C1 (pure goethite) and C5: (1.93 and 2.08–2.09 Å) and the values agree to within ± 0.02 Å with the average distances Fe-O and Fe-OH obtained by the Rietveld simulation procedure (calculated distances Fe-O = 1.949 and 1.952 Å and Fe-OH = 2.095 and 2.099 Å for C1 and C5, respectively). A two-shell model was used to fit the Fe-Fe,Cr links.[1] The resulting first Fe-Me distance remains essentially constant (3.03 ± 0.02 Å), but the distance Fe-Me corresponding to the second peak increases from 3.37 ± 0.03 Å in C1 and to 3.40 ± 0.03 Å in C5 (see Table 6). The second peak distance is close to the weighted average of the E and DC distances from Rietveld simulation (see Table 4). Rietveld analysis demonstrates that E decreases and DC increases, and the position of the mixed EXAFS signal results from the weighed contribution of both signals, the trend being determined by the behavior of DC. In C5, the Fe-(Cr,Fe) (E+DC) distance is appreciably longer than the corresponding Fe-Fe distance in C1. This change influences little the average value obtained by Rietveld methods.

[1] A three-shell model was also used (not shown). A better description of the low frequency beat is thus obtained, but the derived distances are affected by large errors. We believe that the data warrant only a two-shell model, with an average mixed signal of E + DC.

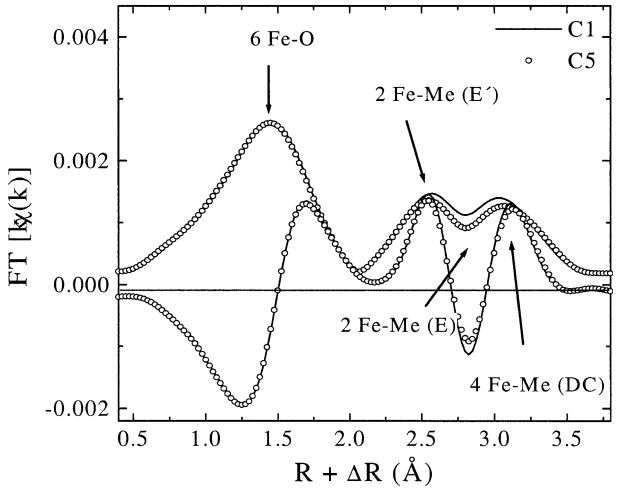

Fig. 7. Fourier transform (FT, modulus and imaginary part) for samples C1 and C5.

Table 6. EXAFs parameters.[a]

Sample	Shell	CN	R (Å)	σ^2 (Å^2)	ΔE (eV)	Residual
Fe K-edge						
C1	Fe-O	3	1.93	0.003	−0.8	14.2
		3	2.08	0.005		
	Fe-Me	2	3.03	0.003	0.5	12.8
		6	3.37	0.012		
C5	Fe-O	3	1.93	0.004	−1.6	14.5
		3	2.09	0.006		
	Fe-Me	2	3.03	0.004	1.9	15.5
		6	3.40	0.015		
Cr K-edge						
C2	Cr-O	6	1.99	0.004	−0.6	15.4
C3		6	1.99	0.004	−0.4	16.3
C4		6	1.99	0.004	−0.2	16.0
C5		6	1.99	0.004	−0.2	16.2
C5[b]	Cr-Me	2	3.04	0.003	−0.9	21.3
		2	3.26	0.005		
		4	3.50	0.011		

[a] CN = coordination number, R = interatomic distances, σ^2 = Debye-Waller factor, ΔE = difference between the threshold energy (E_0) relative to FEFF phase shift function. Uncertainties are estimated to be ± 0.02 Å for shells one to three, uncertainty for shell four is estimated to be ± 0.03 Å. Fits were performed by fixing the CN to their crystallographic values.

[b] An alternative method was used for fitting the Cr-Me shells in C5, the individual CN values and a single σ^2 were varied during the refinement. The fitting yielded: CN1 = 3.3, R1 = 3.05, CN2 = 3.7, R2 = 3.28, CN3 = 3.2, R3 = 3.50, σ^2 = 0.0068 and ΔE = −0.7. This strategy changed the residual (%) from least-squares from 21.3 to 15.8. Residual (%) = $100\ \Sigma\ |k^3\chi_{exp} - k^3\chi_{theo}|/\Sigma\ |k^3\chi_{exp}|$.

3.6. Local Order around Cr(III)

XANES spectra of samples C2 and C5 and grimaldiite at the Cr K-edge are presented in Figure 8. The signals of samples C3 and C4 (not shown) are essentially identical with that of sample C5. In the XANES regime, the multiple scattering of the excited electron is sensitive to the details of the spatial arrangement around the Cr atoms (radial distances, relative orientations, angles, etc.) and strong spectral differences are found for trivalent and hexavalent chromium (Durham, 1988).

The similarity of the edge position in our samples and in grimaldiite confirms the presence of Cr(III) in the Cr-inserted goethites. The small differences just above the edge between the more Cr-diluted (C2) and the other samples are probably associated with the presence of a small quantity of an amorphous Cr oxide in C2 (Fig. 2).

An overlay of the EXAFS spectra is displayed in Figure 9. As in Figure 6, k^3-weighted signals are shown. These signals are

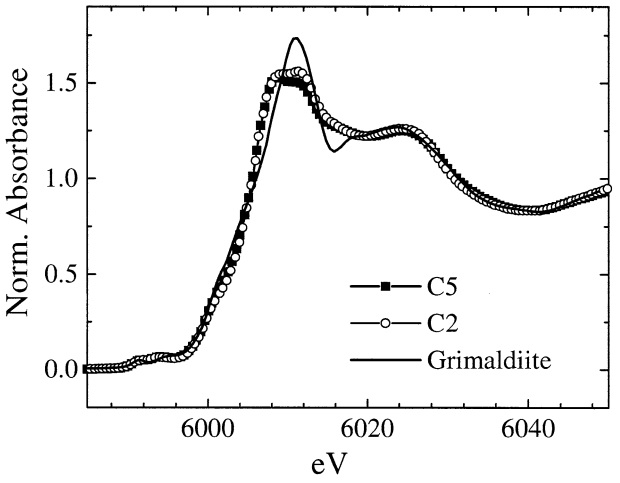

Fig. 8. XANES at the Cr K-edge for C2 and C5 and grimaldiite

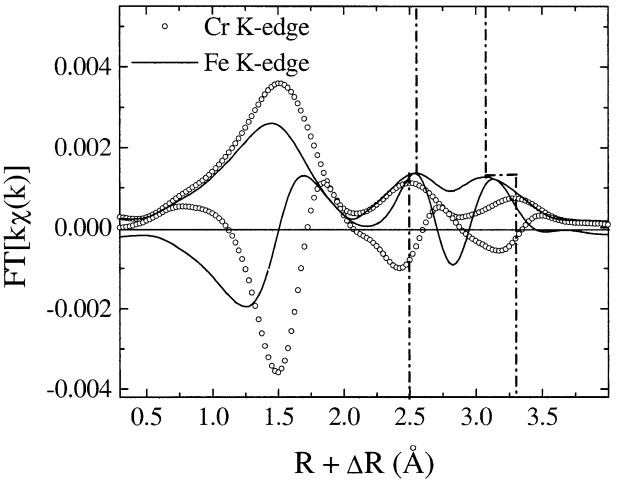

Fig. 10. Comparison of FT[kχ(k)] at the Fe K-edge and at the Cr K-edge for sample C5.

identical for samples C3, C4 and C5; the C2 spectrum is slightly different.

3.7. Comparison of EXAFS Spectra at the Fe K- and Cr K-Edges

Figure 10 compares FT[kχ(k)] at the Fe K- and Cr K-edges for sample C5. The Cr-O peak is stronger than the Fe-O peak indicating a greater coherency of the Cr-O distances. The first metallic shells are slightly displaced around the Cr and the Fe atoms, whereas the third peak is markedly displaced to larger *R*-values at the Cr K-edge.[2] These facts confirm a marked difference in both coordination environments.

Figure 11 compares FT($k^2\chi(k)$) at the Cr-edge for C5 and grimaldiite. For grimaldiite (Nørlund Christensen et al., 1977), three peaks are expected in the range 0.8–4 Å, corresponding to Cr-O_1 (6 O at 1.988 Å), Cr-Me_1 (6 Cr at 2.979 Å) and Cr-O_2 (10 O at an average distance of 3.750 Å). By contrast with the differences noted in the Me-O shells at the Cr- and the Fe-edges in goethites (Fig. 10), in C5 and grimaldiite the FT modulus and the imaginary part of the first shell coincide very precisely. It is concluded that oxygen coordination around Cr in the substituted goethite and grimaldiite are very similar, whereas the coordination around Fe in goethite is appreciably different.

The *R*-values of the second peak, corresponding to the Cr-Me_1 shell, also coincide. The distance corresponding to the third peak in Cr-goethite (Cr-Me_3) may be estimated to be ~3.50 Å, by comparison with the known third peak distance in α-CrOOH (3.750 Å). A residual contribution, Cr-Me_2, is also detected for C5 between Cr-O_1 and Cr-Me_3.

The k^3-weighted Fourier backtransform in the range $3.5 < k < 12.7$ Å^{-1} for C2 to C5 (Cr-O shell) is well reproduced by a simple one-shell model, with 6 O at 1.99–2.00 ± 0.02 Å (the refinement of CN leads to $5.4 < CN < 5.8$). The number of neighbors and distances are almost identical in all samples, demonstrating that the Cr coordination polyhedron is unaltered in the whole series. This fact provides a direct indication that

[2] For an assignment of these distances, see Figure 7.

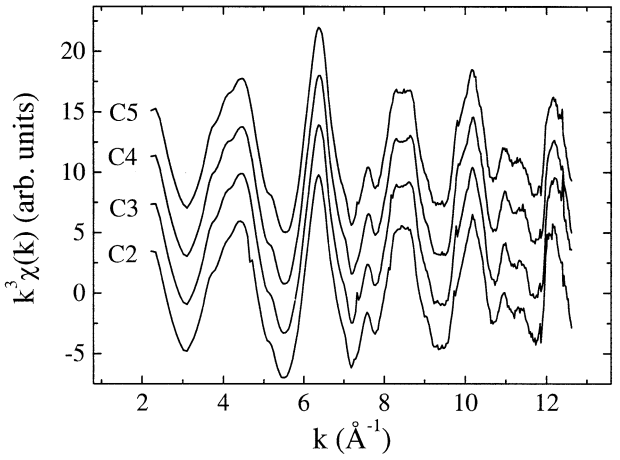

Fig. 9. Comparison of the k^3-weighted spectra for C2 to C5 (Cr K-edge).

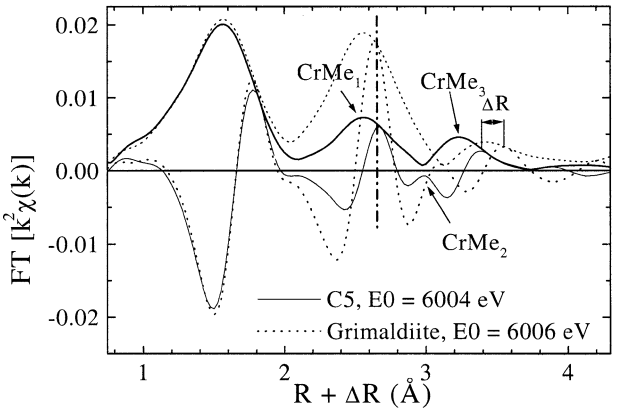

Fig. 11. Comparison between the Fourier transforms of C5 and grimaldiite.

the changes detected by PXRD and Rietveld refinement result from weighted averages of the local distortions introduced by the $Cr(O,OH)_6$ polyhedron in the host structure.

The FT signal in the filtered *R*-window 2.1–3.7 Å was back-transformed and refined in the range $3.5 < k < 12.7$ Å^{-1}. The three metal shell[3] refinement of $k^3\chi(k)$ for sample C5 yielded Cr-Me_1: 3.04 ± 0.02, Cr-Me_2: 3.26 ± 0.02 and CrMe_3: 3.50 ± 0.03 Å (see Table 6). These results together with the value obtained for the refined Cr-O distance, confirm the differences between the Fe and the Cr shells (see Table 5).

3.8. Structural Characteristics of MeOOH (Me = Fe, Cr)

All known phases MeOOH contain $Me(O,OH)_6$ polyhedra, with various degrees of distortion. In goethite, the two opposite staggered triangular faces FeO_3 and $Fe(OH)_3$ are characterized, respectively, by shorter Fe-O distances (two of 1.944(2) and one of 1.960(3) Å, average 1.949 Å) and larger Fe-OH distances (two of 2.092(2) and one of 2.101(3) Å, average 2.095 Å).[4] The distortion of the octahedron can be simply attributed to the different formal charges of the two sets of O ligands. The same situation has been reported for natural samples (Szytula et al., 1968), albeit in this case the spread of distances in each set is smaller.

The distortion of the $Fe(O,OH)_6$ polyhedra in lepidocrocite (Christensen and Nørlund Christensen, 1978) and akaganeite (MacKay, 1960) is again due to the existence of distinct O^{2-} and OH^- ligands; the reader is referred to the original papers for a more detailed discussion of the shape of these polyhedra. Only in the case of δ-FeOOH, feroxyhyte, Patrat et al. (1983) reported regular $Fe(O,OH)_6$ polyhedra. However, Drits et al. (1993) have shown that a better structural model for feroxyhyte involves distorted octahedra, the Fe atoms being displaced from the center of the polyhedra.

By contrast, the $Cr(O,OH)_6$ octahedra in grimaldiite, α-CrOOH (Nørlund Christensen et al., 1977; Ichikawa et al., 1999), are characterized by a single Cr-O distance[5] (reported values range from 1.988 to 1.972 Å, O-Cr-O angles from 82.68 to 97.32°). In this case, H atoms are located half way between two O atoms of adjacent corners. Thus, it may be interpreted that the Cr-O interactions determine the basic features of the structural frame, and H atoms accommodate to yield slightly angularly distorted $Cr(O,OH)_6$ octahedra that can be described as $Cr(OH_{0.5})_6$.

The coordination polyhedron in guyanaite (β-CrOOH) is more distorted (Pernet et al., 1997), with a larger spread in Cr-O distances, but the angular distortion is also small (O-Cr-O angles between 82.33 and 93.30°).

The distances and angles derived from the Rietveld data shown in Table 4, are weighted averages of a set of distinct atomic distances and angles. In going from C1 to C5, the spread in bond lengths of the $Me(O,OH)_6$ polyhedra decreases. Average Me-O distances change from 1.944(2) and 1.959(4) Å to 1.949(4) and 1.953(3) Å; average distances Me-OH also change accordingly, from 2.092(3) and 2.101(3) Å to 2.099(2) and 2.102(2) Å. These changes, and the small variation in the Me-O-Me angle (from 124.0(1) to 124.2(1)°) produce the observed increment in the DC distance (see Table 5 and Fig. 5). The variation in distances and the decrease in the angular distortion of the octahedron (the Me-O-Me angle goes from 102.1(2) to 101.2(2) and the Me-OH-Me angles go from 92.6(1) to 91.9(1) and from 104.2(1)° to 103.2(2)°), also account for the decrease of the E and E′ distances.

Table 4 shows that the atomic coordinates do not change much; however, the modest changes in x(Fe,Cr) and y(Fe,Cr) (samples C1 to C5) suffice to define trends in Me-Me distances.

Within experimental error, EXAFS results at the Fe K-edge are in agreement with Rietveld data: three average distances Fe-O at 1.93 Å (Fe-O) and three average distances at 2.08–2.09 Å (Fe-OH). The data provided at the Cr K-edge on the other hand gives direct evidence of the different environment of the $Cr(O,OH)_6$ unit, only one Cr-O distance being observed at 1.99 ± 0.02 Å. Thus, it can be expected that the average Me-O distances in substituted goethites must increase with Cr content, whereas the average Me-OH distances should decrease. Angular distortions arise, affecting Me-O(H)-Me and Me-O-Me angles in different fashion; these distortions in turn define the behavior of the various Me-Me distances. Upon substitution, the E distance (across an edge containing two OH groups) decreases, the DC distance (across an edge containing two O groups) increases. The change in E′ is not so noticeable because of canceling changes in Me-OH and Me-O bonds. It may be concluded that the occurrence of the more regular $Cr(OH_{0.5})_6$ polyhedra defines the trends in the average E, E′ and DC distances discussed above.

As noted, the second shell distance at the EXAFS Fe K-edge assigned to E′ coincides with the average Rietveld value, and does not change upon substitution. The third shell distance (E + DC linkages) increases from 3.37 to 3.40 Å; comparison with the data in Table 5 shows that this trend seems to be dominated by the changes in DC when Cr substitutes for Fe.

At the Cr K-edge, the E′ distance is similar to that in the Fe K-edge (3.03 vs 3.04 Å). The signals due to E and DC are now clearly separated. E (Cr-Me) is slightly shorter than the Rietveld E value (3.26 vs. 3.29 Å), whereas DC (Cr-Me) is larger than the Rietveld distance (3.50 vs. 3.45 Å). It is thus clear that EXAFS traces the origin of the average Rietveld trends to the differences in the individual shells around Fe and Cr.

4. CONCLUSIONS

Simultaneous use of XAS and Rietveld refinement of XRD data permits a complete explanation for the changes observed locally and in the long range ordering (cell parameters) when Cr^{3+} substitutes for Fe^{3+} in goethite. Even though long-range changes observed in the substituted samples must be traced to local changes in the coordination polyhedron of the individual metal atoms, complex changes in the various interatomic distances and angles may result in deceivingly simple long-range

[3] In this case a three-shell model was used because the three Cr-Me shells are farther apart around Cr than around Fe.
[4] Distances calculated from the refined atomic parameters obtained in the first part of this work.
[5] Although the Cr-O distances reported by Nörlund Christensen and by Ichihawa differ, both authors find that only one distance characterizes the coordination polyhedron.

trends. These trends are therefore of limited value as probes for the atomic scale changes. XAS data on the other hand provide direct information on the fundamental, atomic-scale changes.

Acknowledgments—This work was supported by LNLS (proposal XAS 437/99) and FAPESP (PROC. N° 95/06439-4 and 99/02688-0), and by grants TX80 and I015 from the University of Buenos Aires. We acknowledge Alain Manceau and two anonymous reviewers for constructive comments that enhanced the clarity of this manuscript. We also thank M. S. Netto for stimulating discussions. MAB is member of CONICET.

Associate editor: D. J. Vaughan

REFERENCES

Baes C. F. and Mesmer R. E. (1976) The Hydrolysis of Cations. Wiley.

Blesa M. A. and Matijevic E. (1989) Phase transformation of iron oxides, oxohydroxides, and hydrous oxides in aqueous media. *Adv. Colloids Interface Sci.* **29,** 173–221.

Blesa M. A., Morando P. J., and Regazzoni A. E. (1994) Chemical Dissolution of Metal Oxides. CRC Press.

Charlet L. and Manceau A. (1991) X-ray absorption spectroscopic study of the sorption of the Cr(III) at the oxide-water interface. *J. Colloid Interface Sci.* **148,** 443–458.

Christensen H. and Nørlund Christensen A. (1978) Hydrogen bonds of γ-FeOOH. *Acta Chem. Scand.* **A32,** 87–88.

Cornell R. M. and Schwertmann U. (1996) The Iron Oxides: Structure, Properties, Reactions, Occurrence and Uses. VHC.

Dollase W. A. (1986) Corrections of intensities for preferred orientations in powder diffractometry: Applications of the March Model. *J. Appl. Crystallogr.* **19,** 267–272.

Domingo Pascual C., Rodríguez Clemente R., and Blesa M. A. (1994) Morphological properties of α-FeOOH, γ-FeOOH and Fe_3O_4 obtained by oxidation of aqueous Fe(II) solutions. *J. Colloid Interface Sci.* **165,** 244–252.

Drits V. A., Sakharov B. A., and Manceau A. (1993) Structure of feroxyhyte as determined by simulation of X-ray diffraction curves. *Clay Min.* **28,** 209–222.

Durham P. J. (1988) Data Analysis. In *X-ray Absorption: Principles, Applications, Techniques of EXAFS, SEXAFS and XANES* (eds. D. C. Koningsberger and R. Prins), pp. 54–84. Wiley.

Faust S. D. and Aly O. S. (1981) Chemistry of Natural Waters. Butterworth.

Hazemann J. L., Manceau A., Sainctavit Ph., and Malgrange C. (1992) Structure of the α-$Fe_xAl_{1-x}OOH$ solid solution. *Phys. Chem. Min.* **19,** 25–38.

Ichikawa M., Gustafsson T., Olovsson I. and Tsuchida T. (1999) Powder neutron-diffraction profile analysis of zero-dimensional H-bonded crystal $HCrO_2$. *J. Phys. Chem. Solids* 1875–1880.

Larson A. C. and Von Dreele R. B. (1994) General structure analysis system (GSAS). Report LAUR 86-748. Los Alamos National Laboratory.

Lewis D. G. and Schwertmann U. (1979) The influence of Al on iron oxides. Part III. Preparation of Al goethites in 1 M KOH. *Clay Min.* **23,** 115–126.

MacKay A. L. (1960) β-Ferric oxyhydroxide. *Min. Mag.* **32,** 545–557.

Manceau A. and Combes J. M. (1988) Structure of Mn and Fe oxides and oxyhydroxides: A topological approach by EXAFS. *Phys. Chem. Min.* **15,** 283–295.

Manceau A. and Drits V. A. (1993) Local structure of ferrihydrite and feroxyhyte by EXAFS spectroscopy. *Clay Min.* **28,** 165–184.

Manceau A., Gorshkov A. I., and Drits V. A. (1992a) Structural chemistry of Mn, Fe, Co, and Ni in manganese hydrous oxides: Part I. Information from XANES spectroscopy and electron and X-ray diffraction. *Am. Mineral.* **77,** 1133–1143.

Manceau A., Gorshkov A. I., and Drits V. A. (1992b) Structural chemistry of Mn, Fe, Co, and Ni in manganese hydrous oxides: Part II. Information from EXAFS spectroscopy. *Am. Mineral.* **77,** 1144–1157.

Manceau A., Schlegel M. L., Musso M., Sole V. A., Gauthier C., Petit P. E., and Trolard F. (2000) Crystal chemistry of trace elements in natural and synthetic goethite. *Geochim. Cosmochim. Acta* **64,** 3643–3661.

Martin F., Ildefonse Ph., Hazemann J. L., Noack Y., Grauby O., Beziat D., and de Parseval Ph. (1997) Gallium crystal chemistry in synthetic goethites. *J. Phys IV* **7 (***C2***),** 821–822.

McBride M. B. (1994) Environmental Chemistry of Soils. Oxford University Press.

Milton C., Appleman D. E., Appleman M. H., Chao E. C. T., Guttita F., Dinnin J. D., Dwornik E. J., Ingram B. L. and Rose H. J. Jr. (1976) Merumite, a complex assemblage of chromium minerals from Guyana. Prof. Paper 887. Geological Survey.

Moore J. W. and Ramamoorthy S. (1984) Chromium. In *Heavy Metals in Natural Waters* (ed. R. S. De Santo), pp. 58–76. Springer.

Nørlund Christensen A., Hansen P., and Lehmann M. S. (1977) Isotope effects in the bonds of α-CrOOH and α-CrOOD. *J. Solid State Chem.* **21,** 325–329.

Norris K. and Taylor R. M. (1961) The isomorphous replacement of iron by aluminium in soil goethites. *J. Soil Sci.* **12,** 294–306.

Norris K. and Rosser H. (1983) Mineral phosphate. In *Soils: An Australian Viewpoint* (ed. CSIRO Division of Soils), pp. 335–361. CSIRO, Melbourne.

Parkman R. H., Charnock J. M., Bryan N. D., Livens F. R., and Vaughan D. J. (1999) Reactions of copper and cadmium ions in aqueous solution with goethite, lepidocrocite, mackinawite and pyrite. *Am. Mineral.* **84,** 407–419.

Patrat G., De Bergevin F., Pernet M., and Joubert J. C. (1983) Structure locale de δ-FeOOH. *Acta Crystallogr. B* **39,** 165–170.

Pernet M., Berthet-Colominas C., Alario-Franco M. A., and Christensen A. N. (1977) Etude par diffraction neutronique de l'oxyhydroxyde de chrome beta-CrOOH. *Phys. Stat. Solidi* 81–88.

Rehr J. J., Mustre de Leon J., Zabinski S. I., and Albers R. C. (1991) Theoretical X-ray absorption fine structure standards. *J. Am Chem. Soc.* **113,** 5135–5145.

Ressler T. (1997) Winxas: A new software package not only for the analysis of energy-dispersive XAS data. *J. Phys. IV* **7 (***C2***),** 269–270.

Rietveld H. M. (1969) A profile refinement method for nuclear and magnetic structures. *J. Appl. Crystallogr.* **2,** 65–71.

Sayers D. E. and Bunker B. A. (1988) Data analysis. In *X-ray Absorption: Principles, Applications, Techniques of EXAFS, SEXAFS and XANES* (eds. D. C. Koningsberger and R. Prins), pp. 211–253. Wiley.

Scheinost A. C., Stanjek H., Schulze D., Gasser U., and Sparks D. (2001) Structural environment and oxidation state in goethite-groutite solid solutions. *Am. Min.* **86,** 139–146.

Schulze D. G. and Schwertmann U. (1984) The influence of aluminum on iron oxides. X. Properties of Al-substituted goethies. *Clay Min.* **19,** 521–539.

Schwertmann U. (1988) Occurrence and formation of iron oxides in various pedoenvironments. In *Iron in Soils and Clay Minerals* (eds. J. W. Stucki, B. A. Goodman, and U. Schwertmann), pp. 267–302. ASI Series 217. NATO.

Schwertmann U. and Cornell R. M. (1991) Iron Oxides in the Laboratory: Preparation and Characterization. VHC.

Schwertmann U. and Taylor R. M. (1989) Iron oxides. In *Minerals in Soil Environments* 2nd (eds. J. B. Dixon and S. B. Weed), pp. 379–439. Soil Science Society of America.

Schwertmann U., Gasser U., and Sticher H. (1989) Chromium-for-iron substitution in synthetic goethites. *Geochim. Cosmochim. Acta* **53,** 1293–1297.

Sileo E. E., Alvarez M., and Rueda E. H. (2001) Structural studies on the manganese for iron substitution in the synthetic goethite-jacobsite system. *Int. J. Inorg. Mat.* **3,** 271–279.

Spadini L., Manceau A., Schindler P. W., and Charlet L. (1994) Structure and stability of Cd^{2+} surface complexes on ferric oxides. 1. Results from EXAFS spectroscopy. *J. Colloid Interface Sci.* **168,** 73–86.

Stephens P. W. (1999) Phenomenological model of anisotropic broadening in powder diffraction. *J. Appl. Crystallogr.* **32,** 281–289.

Stiers W. and Schwertmann U. (1985) Evidence for manganese substitution in synthetic goethite. *Geochim. Cosmochim. Acta* **49,** 1909–1911.

Szytula A., Burewicz A., Dimitrijevic Z., Krasnicki S., Rzany H., Todorovic J., Wanic A., and Wolski W. (1968) Neutron diffraction studies of α-FeOOH. *Phys. Stat. Solidi* **26,** 429–434.

Thompson P., Cox D. E., and Hastings J. B. (1987) Rietveld refinement of Debye-Scherrer synchrotron X-ray data from Al_2O_3. *J. Appl. Crystallogr.* **20,** 79–83.

Tolentino H. C. N., Ramos A. Y., Alves M. C. M., Barrea R. A., Tamura E., Cezar J. C., and Watanabe N. (2001) A 2.3 to 25 keV XAS beam line at the LNLS. *J. Synchrotron Radiat.* **8,** 1040–1046.

Wolska E. and Schwertmann U. (1989) Nonstoichiometric structures during dehydroxylation of goethite. *Z. Kristallogr.* **189,** 223–237.